Published in final edited form as:
Cancer. 2010 November 1; 116(21): 4980–4990. doi:10.1002/cncr.25426.

Dasatinib Induces Autophagic Cell Death in Human Ovarian Cancer*

Xiao-Feng Le[1,¶], **Weiqun Mao**[1], **Zhen Lu**[1], **Bing Z. Carter**[2], and **Robert C. Bast Jr**[1,¶]

[1]Department of Experimental Therapeutics, University of Texas M. D. Anderson Cancer Center, Houston, Texas, USA

[2]Department of Stem Cell Transplantation & Cellular Therapy, University of Texas M. D. Anderson Cancer Center, Houston, Texas, USA

Abstract

BACKGROUND—Dasatinib, an inhibitor of Src/Abl family kinases, can inhibit tumor growth of a number of solid tumors. However, the effect and mechanism of action of dasatinib in human ovarian cancer cells remains unknown.

METHODS—Dasatinib-induced autophagy was determined by acridine orange staining, punctate localization of GFP-LC3, LC3 protein blotting and electron microscopy. Significance of Beclin-1, AKT and Bcl-2 in dasatinib-induced autophagy and growth inhibition was assayed by small interfering RNA silencing and/or overexpression of gene of interest.

RESULTS—Dasatinib inhibited cell growth by inducing little apoptosis, but substantial autophagy in SKOv3 and HEY ovarian cancer cells. In vivo studies showed dasatinib inhibited tumor growth and induced both autophagy and apoptosis in a HEY xenograft model. Knockdown of Beclin 1 and Atg12 expression with their respective siRNAs diminished dasatinib-induced autophagy, whereas knockdown of p27Kip1 with specific siRNAs did not. shRNA knockdown of Beclin-1 expression reduced dasatinib-induced autophagy and growth inhibition. Dasatinib reduced the phosphorylation of AKT, mTOR, p70S6K and S6 kinase expression. Constitutive expression of AKT1 and AKT2 inhibited dasatinib-induced autophagy in both HEY and SKOv3 cells. Dasatinib also reduced Bcl-2 expression and activity. Overexpression of Bcl-2 partially prevented dasatinib-induced autophagy.

CONCLUSIONS—We conclude that dasatinib induces autophagic cell death in ovarian cancer that partially depends on Beclin-1, AKT and Bcl-2. These results may have implications for clinical use of dasatinib.

Keywords

Dasatinib; autophagy; ovarian cancer; Beclin 1; AKT; Bcl-2

*This work was supported by the Anne and Henry Zarrow Foundation

¶To whom correspondence should be addressed: Department of Experimental Therapeutics, the, University of Texas M. D. Anderson Cancer Center, Unit 354, phone: 713-745-4353, xfle@mdanderson.org (XFL) or phone: 713-792-7743, rbast@mdanderson.org (RCB).

CONFLICT OF INTEREST DISCLOSURES

The authors declare no conflict of interest.

INTRODUCTION

Dasatinib, a dual inhibitor of Src and Abl tyrosine kinase, was approved by FDA for second-line treatment of chronic myelogenous leukemia[1, 2]. Recently, a number of pre-clinical studies have demonstrated that dasatinib inhibits growth of a variety of solid tumors including breast, prostate, brain, skin, bone, soft tissues, lung, head & neck, colon, and pancreatic cancers [1–7]. Several mechanisms underlie dasatinib-induced suppression of leukemia and solid tumors including G1 arrest of the cell cycle[1, 4, 7], induction of apoptosis [1–4, 7], and inhibition of cell migration/invasion/metastasis [1–8]. However, the effect of dasatinib and the role of autophagy, a type II programmed cell death, in dasatinib-treated ovarian cancer cells has not been reported.

Autophagy is an intracellular degradative mechanism for eliminating damaged organelles and long lived proteins[9, 10]. The process of autophagy can be divided into following steps: signaling initiation, membrane nucleation, vesicle elongation, autophagosome formation, autophagolysome formation and content degradation[11]. Autophagosomes are defined ultrastructurally as intracellular, double-membraned vesicles that contain damaged organelles and proteins and membrane-bound protein called microtubule-associated protein light chain 3-II (LC3-II). LC3-II is modified from LC3-I by cleavage and phosphatidylethanolamine at the C-terminus and binds tightly to autophagosomal membrane [12]. The amount of LC3-II is correlated with the extent of the autophagosome formation[13]. Level of p62/SQSTM1 (p62), a multifunctional protein that targets proteins to degradation by proteasomes and autophagy, is also correlated with the extent of the autophagosome formation [14]. Intact and increased autophagy function decreases p62 protein [14].

The phosphoinositide-3 kinase and mammalian target of rapamycin (mTOR) kinase pathways play major roles in regulating the formation of autophagosomes [9, 10]. A series of proteins encoded by autophagy genes (Atg) participate and execute the process of autophagy [9, 10]. Beclin 1 (Atg6), a Bcl-2 interacting protein, plays a role in autophagy induction [15]. In addition, Beclin 1, Atg14, Vps34, and Vps15 form a lipid kinase complex that engages vesicle nucleation [16]. Atg5, Atg12 and LC3 promote vesicle elongation [17].

Cells induce autophagy as a mean of survival by increasing the turnover of intracellular components [18]. In prolonged adverse conditions, progressive cellular atrophy may lead to type II programmed cell death [18]. Whether autophagy promotes cancer cell survival or produces type II programmed cell death largely depends on the nature of environmental stress and cancer cell context [9, 10, 19–21]. Bcl-2 not only plays a negative role in apoptosis, but also inhibits Beclin-1-dependent autophagy [15, 22]. Therefore, levels of Bcl-2 may influence autophagy process via Beclin-1.

In this report, dasatinib was surprisingly found to induce significant autophagy, rather than apoptosis, in human ovarian cancer cells. We have documented the evidence of dasatinib-induced authophagy in ovarian cancer cells both in vitro and in vivo by a number of methods.

MATERIALS AND METHODS

Antibodies and Reagents

Antibodies recognizing phospho-Src (Y416), total Src and AKT2 were purchased from Upstate-Millipore (Billerica, MA). p27Kip1 antibody was purchased from BD Biosciences (San Diego, CA). Antibodies against p-Akt-Ser473, total AKT, p-mTOR, Beclin 1, Atg12 and p62 were purchased from Cell Signaling Technology (Beverly, MA). Anti-LC3 was provided by Drs. N. Mizushima and T. Yoshimori (National Institute for Basic Biology,

Okazaki, Japan). An antibody to GAPDH was obtained from MBL International (Woburn, MA). siRNAs targeted to p27Kip1, Beclin 1, and Atg12 were from Dharmacon (Lafayette, CO) or Ambion (Austin, TX). Transfection reagents used were LipofectAMINE-2000 from Invitrogen (Grand Island, NY) and DharmaFECT #4 (DF4) from Dharmacon (Lafayette, CO). Dasatinib (Bristol-Myers Squibb, Princeton, NJ) was purchased from Pharmacy Division of M. D. Anderson Cancer Center and dissolved in DMSO. A myristoylated AKT1 and AKT2 were kindly provided by Dr. Gordon B. Mills (M. D. Anderson Cancer Center, Houston, TX). pUC-CAGGS-Bcl-2 plasmid was kindly provided by Dr. Y. Tsujimoto at Osaka University Graduate School of Medicine, Osaka, Japan. A piMARK vector was provided by Dr. Taro Q.P. Uyeda at National Institute of Advanced Industrial Science & Technology, Ibaraki, Japan. A reporter construct containing the Bcl-2 promoter (pBcl-2-Luc) was kindly provided by Dr. Haojie Huang at University of Minnesota (Minneapolis, MN).

Cell Growth Assay

A crystal violet cell growth assay was used to assess anchorage-dependent cell proliferation in 96-well cell culture microplates as described previously 23. Colony-formation assay was performed in 6-well cell culture plates. SKOv3 and HEY cells (both cell lines have been verified by the G-banding karyotyping) were seeded at 1000 and 500 cells per well in triplicate and incubated overnight at 37°C. Cells were treated with either DMSO or dasatinib (300 nM for SKOv3 cells and 150 nM for HEY cells) for 14 days. Cells were fixed in 1% glutaraldehyde, and stained with 0.5% crystal violet (Sigma) in methanol. Colonies with more than 30 cells were counted under an inverted microscope at low magnification. Growth recovery experiments were carried out in similar conditions to colony formation assay. Washout cells were washed with complete media for 2 times first and refilled with complete media after 72h treatment of dasatinib. Instead of counting the colonies, microplate reader was used to quantitate the cell numbers.

Establishment of Stable Ovarian Cancer Subclones

For overexpressing GFP-LC3 and Bcl-2, HEY or SKOv3 cells were co-tranfected with pGFP-LC3 24, or pUC-CAGGS-Bcl-2 25, and pcDNA3.1 (Invitrogen) by Lipofectamine 2000 according to the manufacturer's instructions. Stable clones were selected with G418. For expressing shBECN1, two oligos designed to target Beclin 1 sequence at agaactacaaacgctgttt were synthesized (Sigma-Genosis, Woodland, TX), annealed, and cloned into a piMARK vector 26. The sequences of the two oligos were: forward - 5'-caccagaattatagacgctgtttacgtgtgctgtc cgtaaacagcgtttgtagttcttttt-3', reverse - 5'-gcataaaaagaactacaaacgctgtttacggacagcacacgtaaacagcgtct ataattct-3'. Resultant pishBECN1 construct was verified by DNA sequencing. Stable clones were selected with blastcidin.

siRNA and Plasmid Transfection

HEY or SKOv3 cells were seeded on 6-well culture plates and transfected with control, Beclin 1 or Atg12 siRNAs using the DF4 reagent (Dharmacon). A mixture of siRNA (50 nM final concentration) and transfection reagents were incubated for 20 min. Empty vector pcDNA3.1, or pGFP-LC3, or myristoylated AKT1 and AKT2 was transfected with Lipofectamine 2000.

Cell Cycle Distribution and Immunoblot Analysis

Distribution of cells in the sub-G1, G1, S, and G2/M phases of the cell cycle, and Western blot analysis was measured as described previously 27.

Quantitative Reverse-transcription Polymerase Chain Reaction (QRTPCR) Analysis

QRTPCR was performed with an ABI Prism 7900HT Sequence Detection System using SYBR Green universal PCR master mix (ABI, Foster City, CA) as described previously 28. Oligonucleotide sequences of the primer sets used were: human Bcl-2 (forward 5'-gggtacgataaccgggagat-3', reverse 5'- ctgaagagctcctccaccac-3'); human GAPDH: forward (5'-cgtcttcaccaccatggaga-3', reverse 5'-cggccatcacgccacagttt-3'). The melting curves were used to ensure there was not any non-specific amplification.

Apoptotic Assay

Caspase 3/7 activity was measured after dasatinib treatment with a Caspase-Glo 3/7 kit from Promega (Madison, WI) according to the manufacturer's instruction. POLARstar OPTIMA (BMG Labtech, Offenburg, Germany) was used to determine the luminescent units of caspase activity.

Luciferase Reporter Assays

HEY cells were seeded on 12-well culture plates in triplicate and first tranfected with a reporter construct containing the Bcl-2 promoter (pBcl-2-Luc) 29 for 48 hrs. Cells were then treated with dasatinib at different concentrations for another 24 hrs. Relative luminescence units (RLU) were normalized with protein concentrations in each sample and final values of RLU were expressed as RLU per μg protein per ml.

HEY Xenografts in Nude Mice

10^6 HEY cells in 0.1 ml PBS were subcutaneously implanted into the flanks of 4-week-old female athymic nu/nu mice (ERO Animal Facility, M. D. Anderson Cancer Center). Five mice per group were used for each treatment. Once the tumors became palpable (mean size of 0.3 mm^3 on day 4 after inoculation), mice were divided into two groups and treated intraperitoneally (ip) with either dasatinib (10 mg/kg) or vehicle DMSO five times a week. Treatment was continued for two and half weeks. Tumors were collected immediately after sacrifice and fixed for electron microscopy as described below. The tumor volume in mm^3 was calculated as described previously 30. Experiments with nude mice were repeated two times with similar results. The results are presented as the mean ± standard error for all values. Experiments with nu/nu mice were reviewed and approved by the M. D. Anderson Cancer Center - Institutional Animal Care and Use Committee (IACUC).

Acridine Orange (AO) Staining

AO flow cytometry was used to detect the development of acidic vesicular organelles (AVO) as described before with minor modification 31. Briefly, SKOv3 and HEY cells were treated with or without dasatinib for 24hrs. Cells were then stained with 0.5 μg/mL AO (Molecular Probes, Eugene, OR) in complete medium at 37°C for 15 min, and examined by flow cytometry within 2 hrs.

Confocal Microscopic Analysis of GFP-LC3 Spots

HEY subclones that stably expressed GFP-LC3 or cells that were transiently tranfected with pGFP-LC3 were fixed with 4% formaldehyde after treatment with dasatinib (150nM) for 24 hr. Cells were then washed with PBS, mounted, and examined using a confocal microscope (Olympus FluoView 1000, Olympus Inc, Melville, NY). Digital images were obtained using FluoView 1000 software (Olympus). 200 GFP-LC3 cells that had more than 10 bright punctate GFP-LC3 spots were counted. The percentage of these cells among DMSO- or dasatinib-treated groups was calculated.

Transmission Electron Microscopy

Tissue or cells were fixed overnight at 4°C with a solution containing 3% glutaraldehyde plus 2% paraformaldehyde in 0.1M cacodylate buffer (pH 7.3). Samples were treated with 0.1% cacodylate buffered tannic acid, postfixed with 1% buffered osmium tetroxide for 30 min, and stained en bloc with 1% uranyl acetate. Samples were then dehydrated in increasing concentrations of ethanol, infiltrated, and embedded in LX-112 medium (Electron Microscopic Sciences, Fort Washington, PA). The samples were polymerized in a 70°C oven for two days. Ultrathin sections were cut in a Leica ultracut microtome (Leica, Deerfield, IL), stained with uranyl acetate and lead citrate in a Leica EM Stainer, and examined in a JEOL 1010 transmission electron microscope (JEOL USA, Peabody, MA) at an accelerating voltage of 80 kV. Digital images were obtained using AMT Imaging System (Advanced Microscopy Techniques Co., Danvers, MA).

Statistical Analysis

The results are presented as the mean ± 95% confidence intervals for all values except in vivo studies. A paired Student's *t* tests or ANOVA testing was used to compare the differences among groups, with statistical significance considered if $P \leq 0.05$.

RESULTS

Dasatinib Inhibits Tyrosine Phosphorylation of Src Kinase, Anchorage-dependent Cell Proliferation and Colony Formation of Ovarian Cancer Cells, but Induces Minimal Apoptosis

Tyrosine phosphorylation of Src kinase at site 416 (p-Y416 Src) is critical for its kinase activity 32. Dasatinib profoundly inhibited p-Y416 Src (Fig. 1A). Dasatinib also inhibited anchorage-dependent cell growth of HEY (Fig. 1B) and SKOv3 (Fig. 1C) ovarian cancer cells in a dose-dependent manner. At levels of dasatinib that can be attained in human plasma (~ 250 – 300nM), short-term treatment (72 hr) with dasatinib inhibited growth of HEY cells by 46% (Fig. 1B) and SKOv3 cells by 34% (Fig. 1C). Long-term treatment (14 days) with dasatinib significantly suppressed the ability of both HEY and SKOv3 cells to form colonies by 70% (Fig. 1D). Surprisingly, no significant apoptosis was detected in dasatinib-treated HEY and SKOv3 cells as shown in Figure 1E –1G.

Dasatinib Induces Autophagy in Human Ovarian Cancer Cells in vitro

Acridine orange (AO) is a lysosomotropic agent and is able to stain the acidic vesicular organelles (AVOs) 31. Although AO staining is not restricted to autophagic vesicles, this technique offers a rapid and quantitative method to measure induction of autophagy. Consequently, we have first employed the AO staining and flow cytometric analysis to evaluate dasatinib-treated HEY cells for AVOs. As shown in Figure 2A, dasatinib treatment for 72hr dramatically increased red fluorescence in HEY cells from 5.1% to 81.0%, indicating the induction of AVOs. Similar results were obtained in SKOv3 cells (Data not shown). The effect of dasatinib on endogenous LC3 protein was checked by Western blotting. As shown in Figure 2B, dasatinib decreased LC3-I protein and increased LC3-II in both SKOv3 and HEY cells. Dasatinib concurrently decreased p62 levels (Fig. 2B), consistently with its correlation with autophagy 14. These results were further confirmed by GFP-LC3 fluorescence microscopic analysis. After dasatinib treatment, punctate GFP-LC3 fluorescent spots dramatically increased, while diffuse fluorescence of GFP-LC3 in the cytoplasm and the nucleus disappeared (Fig. 2C). Dasatinib treatment resulted in 57% of HEY cells with punctate LC3, whereas only 8.4% cells with punctuate LC3 in DMSO-treated cells (Fig. 2D). Similar results were also found in SKOv3 cells (Fig. 2E). Finally, dasatinib-induced autophagy was confirmed by transmission electron microscopy. Dasatinib

induced a dramatic increase in autophagosomes (blue arrows) and autophagolysomes (green arrows) in the cytoplasm of both HEY cells (Fig. 2F) and SKOv3 cells (Fig. 2G). In contrast, DMSO-cells exhibited only normal mitochondria and endoplasmic reticulum without autophagic vesicles (Fig. 2F & 2G). No apoptotic features were found in dasatinib-treated HEY and SKOv3 cells. Thus, dasatinib induces typical autophagy in human ovarian cancer cells in vitro.

Dasatinib Inhibits Ovarian Tumor Growth and Induces Autophagy and Apoptosis in Ovarian Cancer Xenografts

To further confirm the ability of dasatinib to induce autophagy, a HEY ovarian cancer xenograft model in nu/nu mice was employed to test the effects of dasatinib in vivo. As shown in Figure 3A, treatment with dasatinib at a dose of 10 mg/kg significantly suppressed the growth of HEY tumors. Ultrastructural analysis of the xenograft tumors collected at day 21 showed autophagosomes (blue arrows) and autophagolysomes (green arrows) in dasatinib-treated tumors (Fig. 3C), but not in DMSO-treated tumors (Fig. 3B). In contrast to the in vitro results, electron microscopic examination of xenograft tumors also showed typical signs of apoptosis such as nuclear condensation and nuclear body in dasatinib-treated tumors (Fig. 3E, red arrows), but not in DMSO-treated tumors (Fig. 3D). These data demonstrate that dasatinib inhibits ovarian tumor growth and induces autophagy and apoptosis in vivo.

Beclin 1 and Atg12 are Critical for Dasatinib-induced Autophagy

Dasatinib was able to induce p27Kip1-dependent G1 arrest of the cell cycle (Data not shown). p27Kip1 has been reported to play a role in autophagy induction in some settings [33, 34]. Therefore, we sought to test whether or not dasatinib-induced autophagy is p27Kip1-dependent. HEY cells were transiently transfected with small interfering RNA (siRNA) targeted to p27Kip1 (p27 siR), control siRNA, or siRNAs targeted to well-known mediators that are required for autophagy induction such as Beclin 1 and Atg 12. As shown in Figure 4A, knockdown of p27Kip1 with p27 siR1 did not reduce dasatinib-induced autophagy. Similar results were achieved with a second p27 siR2 (Data not shown). As expected, downregulation of Beclin 1 or Atg12 with respective siRNAs significantly blocked dasatinib-induced autophagy (Fig. 4A). Effects of p27 siRNA, Beclin 1 siRNA, and Atg12 siRNA used in this study on respective proteins have been demonstrated by Western blotting (Fig. 4B–4D). These results indicate that Beclin 1 and Atg12, but not p27Kip1 are critical for dasatinib-induced autophagy.

Dasatinib-induced Growth Inhibition Partially Depends upon Autophagy Induction

To determine whether dasatinib-induced autophagy is responsible for growth inhibition in ovarian cancer cells, we have chosen to downregulate Beclin 1 as a testing model since it was required in dasatinib-induced autophagy (Fig. 4A). Beclin 1 siRNA sequences were subcloned into piMARK shRNA vector. Two stable sublines that consistently express reduced Beclin 1 levels were selected (Fig. 4E). As shown in Figure 4F, shBECN #46 and #69 cells were more resistant to dasatinib-induced inhibition of cell growth as compared to piMARK control cells. shBECN #46 and #69 cells had lower autophagy induction than the piMARK control in response to dasatinib treatment (Fig. 4G), consistent with the Beclin 1siRNA data. These results suggest that dasatinib-induced autophagy accounts for dasatinib-induced growth inhibition in ovarian cancer cells.

Dasatinib-induced Autophagy Partially Depends on AKT

To investigate the mechanisms of dasatinib-induced autophagy, we have studied the effects of dasatinib on phosphorylation of AKT and mTOR by Western blotting. As shown in

Figure 5A, dasatinib treatment dramatically decreased phosphorylation of AKT and mTOR in both HEY and SKOv3 cells. To confirm the value of decreasing AKT in dasatinib-induced autophagy, HEY cells that stably express AKT1 and AKT2 were produced. AKT1 and AKT2 cells were transiently transfected with GFP-LC3 expression vector, and then treated with dasatinib for 24h. GFP-LC3 punctate was checked by confocal microscope. Overexpression of both AKT1 and AKT2 partially attenuates dasatinib-induced LC3 spots (Fig. 5B). This attenuated effect was associated with decreased inhibition of AKT and mTOR phosphorylation by dasatinib (Fig. 5C). Effects of AKT1 and AKT2 overexpression on dasatinib-induced autophagy was further confirmed in SKOv3 cells by using the flow cytometric AO staining (Fig. 5D). A reverse phase protein array (RPPA) analysis was performed to check the signaling pathways affected by dasatinib. Results confirmed the inhibitory effects of dasatinib on p-AKT and p-mTOR and further showed that downstream targets of AKT and mTOR, p70S6K and S6, were significantly suppressed (Fig. 5E). Therefore, above data indicate that dasatinib-induced autophagy partially depends on AKT pathway.

Dasatinib inhibits Bcl-2 Levels and its Promoter Activity

Anti-apoptotic Bcl-2 binds Beclin 1 and inhibits Beclin 1-dependent autophagy 15, 22, 35. Since dasatinib-induced autophagy is Beclin 1-dependent (Fig. 4), we sought to check the effect of dasatinib on Bcl-2 levels. As shown in Figure 6A, dasatinib markedly suppressed Bcl-2 protein levels illustrated by Western blotting. Dasatinib also reduced Bcl-2 mRNA level as shown by quantitative PCR (Fig. 6B), indicating that dasatinib-induced Bcl-2 downregulation occurred at the level of transcription. Consistent with this conclusion, dasatinib decreased Bcl-2 promoter activity in a dose-dependent manner (Fig. 6C). To further determine the role of Bcl-2 downregulaton in dasatinib-induced autophagy, HEY cells that stably express Bcl-2 were generated. As shown in Figure 6D, overexpression of Bcl-2 partially but significantly blocked dasatinib-induced autophagy in two independent sublines that overexpressed Bcl-2 as demonstrated by AO staining. This result was further confirmed by GFP-LC3 fluorescence analysis. As shown in Figure 6F, Bcl-2-overexpressing HEY cells exhibited less LC3 punctate spots induced by dasatinib treatment than that of control cells, indicating partial blockade of dasatinib-induced autophagy by Bcl-2 expression. Collectively, these results show that dasatinib-induced autophagy partially depends on Bcl-2.

DISCUSSION

While this report is being prepared for publication, a study has just published and shown that dasatinib induces autophagy, but not G1 arrest or apoptosis, in glioma cells 36. Our study presented here not only showed dasatinib-induced autophagy by AO staining and LC3 Western blotting, but also documented it by in vivo study and additional methods including electron microscopy. Our report has also revealed several key molecules and pathway such as Beclin 1, AKT and Bcl-2 that are required for dasatinib-induced autophagy. More importantly, we show that dasatinib-induced autophagy was functionally required for dasatinib-induced inhibition of cell growth.

Results shown by Milano indicate that dasatinib-induced autophagy is independent of the cell cycle G1 arrest 36, consistent with our observations that dasatinib-induced autophagy depended on Beclin 1- and Atg12, but not p27Kip1 in ovarian cancer cells (Fig. 4A). However, there are reports that indicate the role of p27Kip1 in autophagy 33, 34. LKB1-AMPK-dependent phosphorylation of p27Kip1 at Thr 198 (p-T198 p27) is reported to increase p27Kip1 and autophagy induction 34. Our data do not support the role of p27Kip1 in dasatinib-induced autophagy. Interestingly, knockdown of p27Kip1 seems to somehow increase dasatinib-induced autophagy (Fig. 4A). We do not know why p27Kip1 depletion

enhances dasatinib-induced autophagy in HEY cells. We do know that dasatinib does not increase p-T198 p27 and AMPK phosphorylaiton (Data not shown). If p-T198 p27 is required for p27Kip1 to induce autophagy, dasatinib-induced p27Kip1 is unable to induce autophagy. Another possibility is that p27Kip1 expresses parallel or downstream of Src/Abl kinases inhibition. Src/Abl kinases has been indicated in directly regulating p27Kip1 expression 37, 38. Dasatinib-induced p27Kip1 could be directly from inhibition of Src/Abl kinases.

Dasatinib can induce both autophagy and apoptosis in vivo, but only autophagy in vitro in ovarian cancer cells (Fig. 2 & 3). The mechanism(s) underlying this disparity are unknown. It is possible that in vivo environmental conditions such as hypoxia, nutrition insufficiency or deprivation, and immunodefensive system permit dasatinib to induce both type I and type II PCD. Apoptosis induced in HEY xenograft model by dasatinib may result from autophagy-dependent mechanism. Prolonged and massive induction of autophagy is known to lead to autophagic cell death 18. Indeed, Konecny et al reported that dasatinib treatment with higher dose (1 μM) and longer duration (5 days) induced significant apoptosis in ovarian cancer cell lines39. Resveratrol-induced apoptosis was reported to depend on resveratrol-induced autophagy 40. Therefore, dasatinib-induced autophagy and apoptosis may be related and contribute to dasatinib-induced growth inhibition.

Our in vitro and in vivo data showed that dasatinib induces autophagic cell death that accounts for dasatinib-induced growth inhibition in human ovarian cancer cells. Beclin 1, AKT and Bcl-2 are critical mediators of dasatinib-induced autophagy.

Acknowledgments

We are grateful to the Anne and Henry Zarrow Foundation and to Mr. Stuart Zarrow for grants supporting these studies. The High Resolution Electron Microscopy Core Facility, Flow Cytometry Core Facility South Campus, Media Preparation Core Facility and Animal Core Facility were supported by the Core Grant CA16672 from NCI. We thank Drs. N. Mizushima and T. Yoshimori for supplying LC3 antibody and GFP-LC3 vector, Dr. Gordon B. Mills for providing AKT1/AKT2 plasmids, Dr. Y. Tsujimoto for providing Bcl-2 plasmid, Dr. Taro QP Uyeda for supplying the piMARK vector, and Dr. Haojie Huang for providing Bcl-2 promoter construct.

REFERENCES

1. Eustace AJ, Crown J, Clynes M, O'Donovan N. Preclinical evaluation of dasatinib, a potent Src kinase inhibitor, in melanoma cell lines. J Transl Med. 2008; 6:53. [PubMed: 18823558]
2. Tsao AS, He D, Saigal B, et al. Inhibition of c-Src expression and activation in malignant pleural mesothelioma tissues leads to apoptosis, cell cycle arrest, and decreased migration and invasion. Mol Cancer Ther. 2007; 6:1962–1972. [PubMed: 17620427]
3. Shor AC, Keschman EA, Lee FY, et al. Dasatinib inhibits migration and invasion in diverse human sarcoma cell lines and induces apoptosis in bone sarcoma cells dependent on SRC kinase for survival. Cancer Res. 2007; 67:2800–2808. [PubMed: 17363602]
4. Song L, Morris M, Bagui T, Lee FY, Jove R, Haura EB. Dasatinib (BMS-354825) selectively induces apoptosis in lung cancer cells dependent on epidermal growth factor receptor signaling for survival. Cancer Res. 2006; 66:5542–5548. [PubMed: 16740687]
5. Serrels A, Macpherson IR, Evans TR, et al. Identification of potential biomarkers for measuring inhibition of Src kinase activity in colon cancer cells following treatment with dasatinib. Mol Cancer Ther. 2006; 5:3014–3022. [PubMed: 17148760]
6. Nam S, Kim D, Cheng JQ, et al. Action of the Src family kinase inhibitor, dasatinib (BMS-354825), on human prostate cancer cells. Cancer Res. 2005; 65:9185–9189. [PubMed: 16230377]
7. Johnson FM, Saigal B, Talpaz M, Donato NJ. Dasatinib (BMS-354825) tyrosine kinase inhibitor suppresses invasion and induces cell cycle arrest and apoptosis of head and neck squamous cell carcinoma and non-small cell lung cancer cells. Clin Cancer Res. 2005; 11:6924–6932. [PubMed: 16203784]

8. Park SI, Zhang J, Phillips KA, et al. Targeting SRC family kinases inhibits growth and lymph node metastases of prostate cancer in an orthotopic nude mouse model. Cancer Res. 2008; 68:3323–3333. [PubMed: 18451159]
9. Klionsky DJ, Emr SD. Autophagy as a regulated pathway of cellular degradation. Science. 2000; 290:1717–1721. [PubMed: 11099404]
10. Levine B, Kroemer G. Autophagy in the pathogenesis of disease. Cell. 2008; 132:27–42. [PubMed: 18191218]
11. Eskelinen EL. Maturation of autophagic vacuoles in Mammalian cells. Autophagy. 2005; 1:1–10. [PubMed: 16874026]
12. Tanida I, Ueno T, Kominami E. Human light chain 3/MAP1LC3B is cleaved at its carboxyl-terminal Met121 to expose Gly120 for lipidation and targeting to autophagosomal membranes. J Biol Chem. 2004; 279:47704–47710. [PubMed: 15355958]
13. Kabeya Y, Mizushima N, Ueno T, et al. LC3, a mammalian homologue of yeast Apg8p, is localized in autophagosome membranes after processing. Embo J. 2000; 19:5720–5728. [PubMed: 11060023]
14. Mathew R, Karp CM, Beaudoin B, et al. Autophagy suppresses tumorigenesis through elimination of p62. Cell. 2009; 137:1062–1075. [PubMed: 19524509]
15. Pattingre S, Tassa A, Qu X, et al. Bcl-2 antiapoptotic proteins inhibit Beclin 1-dependent autophagy. Cell. 2005; 122:927–939. [PubMed: 16179260]
16. Itakura E, Kishi C, Inoue K, Mizushima N. Beclin 1 forms two distinct phosphatidylinositol 3-kinase complexes with mammalian Atg14 and UVRAG. Mol Biol Cell. 2008; 19:5360–5372. [PubMed: 18843052]
17. Geng J, Klionsky DJ. The Atg8 and Atg12 ubiquitin-like conjugation systems in macroautophagy. 'Protein modifications: beyond the usual suspects' review series. EMBO Rep. 2008; 9:859–864. [PubMed: 18704115]
18. Lum JJ, DeBerardinis RJ, Thompson CB. Autophagy in metazoans: cell survival in the land of plenty. Nat Rev Mol Cell Biol. 2005; 6:439–448. [PubMed: 15928708]
19. Eskelinen EL, Saftig P. Autophagy: A lysosomal degradation pathway with a central role in health and disease. Biochim Biophys Acta. 2009; 1793:664–673. [PubMed: 18706940]
20. Kourtis N, Tavernarakis N. Autophagy and cell death in model organisms. Cell Death Differ. 2009; 16:21–30. [PubMed: 19079286]
21. Levine B, Kroemer G. Autophagy in aging, disease and death: the true identity of a cell death impostor. Cell Death Differ. 2009; 16:1–2. [PubMed: 19079285]
22. Levine B, Sinha S, Kroemer G. Bcl-2 family members: dual regulators of apoptosis and autophagy. Autophagy. 2008; 4:600–606. [PubMed: 18497563]
23. Le XF, McWatters A, Wiener J, Wu JY, Mills GB, Bast RC Jr. Anti-HER2 antibody and heregulin suppress growth of HER2-overexpressing human breast cancer cells through different mechanisms. Clin Cancer Res. 2000; 6:260–270. [PubMed: 10656457]
24. Mizushima N, Yamamoto A, Matsui M, Yoshimori T, Ohsumi Y. In vivo analysis of autophagy in response to nutrient starvation using transgenic mice expressing a fluorescent autophagosome marker. Mol Biol Cell. 2004; 15:1101–1111. [PubMed: 14699058]
25. Ikegaki N, Katsumata M, Minna J, Tsujimoto Y. Expression of bcl-2 in small cell lung carcinoma cells. Cancer Res. 1994; 54:6–8. [PubMed: 8261463]
26. Nagasaki A, Kanada M, Uyeda TQ. A novel shRNA vector that enables rapid selection and identification of knockdown cells. Plasmid. 2007; 58:190–194. [PubMed: 17688947]
27. Le XF, Vadlamudi R, McWatters A, et al. Differential signaling by an anti-p185(HER2) antibody and heregulin. Cancer Res. 2000; 60:3522–3531. [PubMed: 10910064]
28. Le XF, Lammayot A, Gold D, et al. Genes affecting the cell cycle, growth, maintenance, and drug sensitivity are preferentially regulated by anti-HER2 antibody through phosphatidylinositol 3-kinase-AKT signaling. J Biol Chem. 2005; 280:2092–2104. [PubMed: 15504738]
29. Huang H, Cheville JC, Pan Y, Roche PC, Schmidt LJ, Tindall DJ. PTEN induces chemosensitivity in PTEN-mutated prostate cancer cells by suppression of Bcl-2 expression. J Biol Chem. 2001; 276:38830–38836. [PubMed: 11495901]

30. Wen XF, Yang G, Mao W, et al. HER2 signaling modulates the equilibrium between pro- and antiangiogenic factors via distinct pathways: implications for HER2-targeted antibody therapy. Oncogene. 2006; 25:6986–6996. [PubMed: 16715132]

31. Kanzawa T, Bedwell J, Kondo Y, Kondo S, Germano IM. Inhibition of DNA repair for sensitizing resistant glioma cells to temozolomide. J Neurosurg. 2003; 99:1047–1052. [PubMed: 14705733]

32. Smart JE, Oppermann H, Czernilofsky AP, Purchio AF, Erikson RL, Bishop JM. Characterization of sites for tyrosine phosphorylation in the transforming protein of Rous sarcoma virus (pp60v-src) and its normal cellular homologue (pp60c-src). Proc Natl Acad Sci U S A. 1981; 78:6013–6017. [PubMed: 6273838]

33. Komata T, Kanzawa T, Takeuchi H, et al. Antitumour effect of cyclin-dependent kinase inhibitors (p16(INK4A), p18(INK4C), p19(INK4D), p21(WAF1/CIP1) and p27(KIP1)) on malignant glioma cells. Br J Cancer. 2003; 88:1277–1280. [PubMed: 12698196]

34. Liang J, Shao SH, Xu ZX, et al. The energy sensing LKB1-AMPK pathway regulates p27(kip1) phosphorylation mediating the decision to enter autophagy or apoptosis. Nat Cell Biol. 2007; 9:218–224. [PubMed: 17237771]

35. Pattingre S, Levine B. Bcl-2 inhibition of autophagy: a new route to cancer? Cancer Res. 2006; 66:2885–2888. [PubMed: 16540632]

36. Milano V, Piao Y, LaFortune T, de Groot J. Dasatinib-induced autophagy is enhanced in combination with temozolomide in glioma. Mol Cancer Ther. 2009; 8:394–406. [PubMed: 19190119]

37. Chu I, Sun J, Arnaout A, et al. p27 phosphorylation by Src regulates inhibition of cyclin E-Cdk2. Cell. 2007; 128:281–294. [PubMed: 17254967]

38. Grimmler M, Wang Y, Mund T, et al. Cdk-inhibitory activity and stability of p27Kip1 are directly regulated by oncogenic tyrosine kinases. Cell. 2007; 128:269–280. [PubMed: 17254966]

39. Konecny GE, Glas R, Dering J, et al. Activity of the multikinase inhibitor dasatinib against ovarian cancer cells. Br J Cancer. 2009; 101:1699–1708. [PubMed: 19861960]

40. Trincheri NF, Follo C, Nicotra G, Peracchio C, Castino R, Isidoro C. Resveratrol-induced apoptosis depends on the lipid kinase activity of Vps34 and on the formation of autophagolysosomes. Carcinogenesis. 2008; 29:381–389. [PubMed: 18048384]

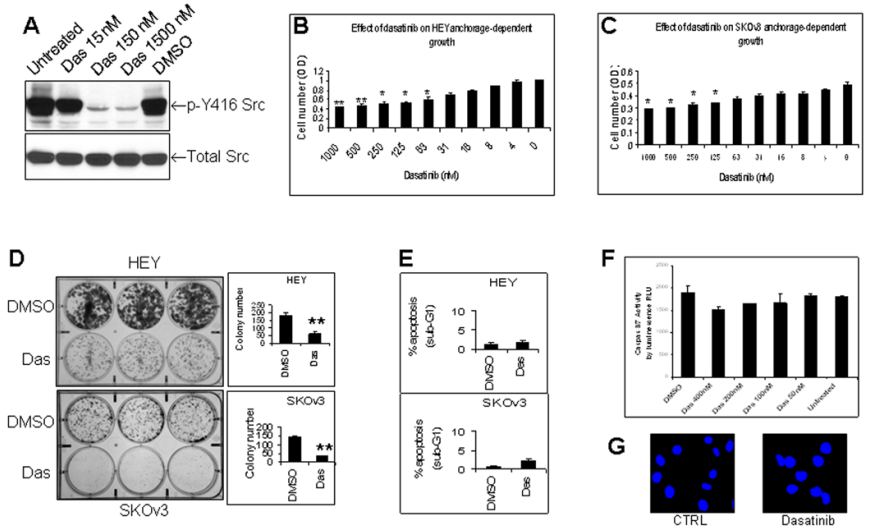

FIGURE 1.

Dasatinib inhibits Src tyrosine phosphorylation, cell proliferation and colony formation of human ovarian cancer cells with minimal induction of apoptosis in vitro. (**A**), Effect of dasatinib (Das) on tyrosine phosphorylation of Src at tyrosine 416. HEY cells were treated with dasatinib or DMSO for 24 hrs and total protein was then extracted for Western blotting. (**B**), Effect of dasatinib on HEY growth. HEY cells were treated with dasatinib for 72 hrs. Crystal violet staining expressed as optical density (OD) was used to measure cell proliferation. *, $P < 0.05$ compared to untreated group. **, $P < 0.01$ compared to untreated group. (**C**), Effect of dasatinib on SKOv3 growth. SKOv3 cells were treated and evaluated as described in Fig. 1B. *, $P < 0.05$. (**D**), Effect of dasatinib on colony formation. HEY and SKOv3 cells were treated with dasatinib for 14 days. **, $P < 0.01$. (**E**), Effect of dasatinib on apoptosis in HEY and SKOv3 cells as determined by Sub-G1 fraction. HEY and SKOv3 cells were treated with dasatinib (150 nM for HEY, 300 nM for SKOv3) for 24 hr. (**F**, **G**), Effect of dasatinib on caspase activity and nuclear morphology. HEY cells were treated with dasatinib for 24 hr. Caspase 3/7 activity (**F**) was expressed as relative luminescence unit (RLU). DAPI was used to stain nuclei (**G**).

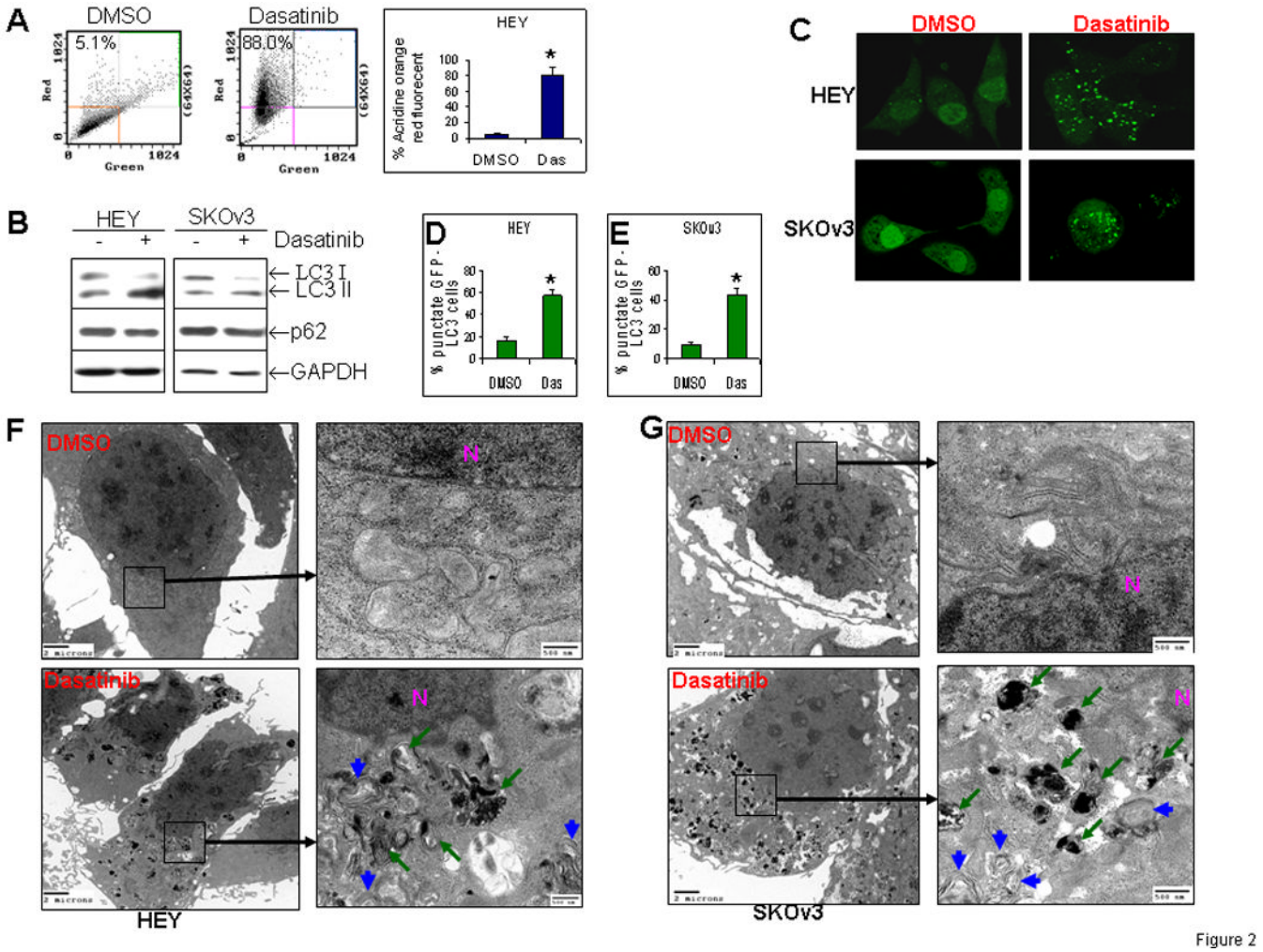

Figure 2

FIGURE 2.

Dasatinib induces autophagy in human ovarian cancer cells in vitro. (**A**), Measurement of dasatinib (Das)-induced autophagy with acridine orange (AO) staining. HEY cells were treated with dasatinib for 72 hrs. AO-stained cells were analyzed by flow cytometry. *, $P < 0.05$. (**B**), Measurement of dasatinib-induced autophagy with Western blotting. HEY and SKOv3 cells were treated as described in Fig. 2A. (**C**), Measurement of dasatinib-induced autophagy with stable subclones that express GFP-LC3. HEY and SKOv3 stable cells were treated with dasatinib for 72 hrs. GFP-LC3 cells with more than 10 bright punctate GFP-LC3 spots were counted and shown as the percentage among DMSO- or Das-treated groups in HEY (**D**) and SKOv3 (**E**) clones. *, $P < 0.05$. (**F**), Measurement of dasatinib-induced autophagy with electron microscopy (EM) in HEY cells. Cells were processed for EM examination as described in Materials and Methods. Two magnifications (4,000× and 25,000×) of ultrastructure are shown. Autophagosomes are indicated by blue arrows and autophagolysomes by green arrows. N indicates the nucleus. (**G**), Measurement of dasatinib-induced autophagy with electron microscopy (EM) in SKOv3 cells as described in Fig. 2F.

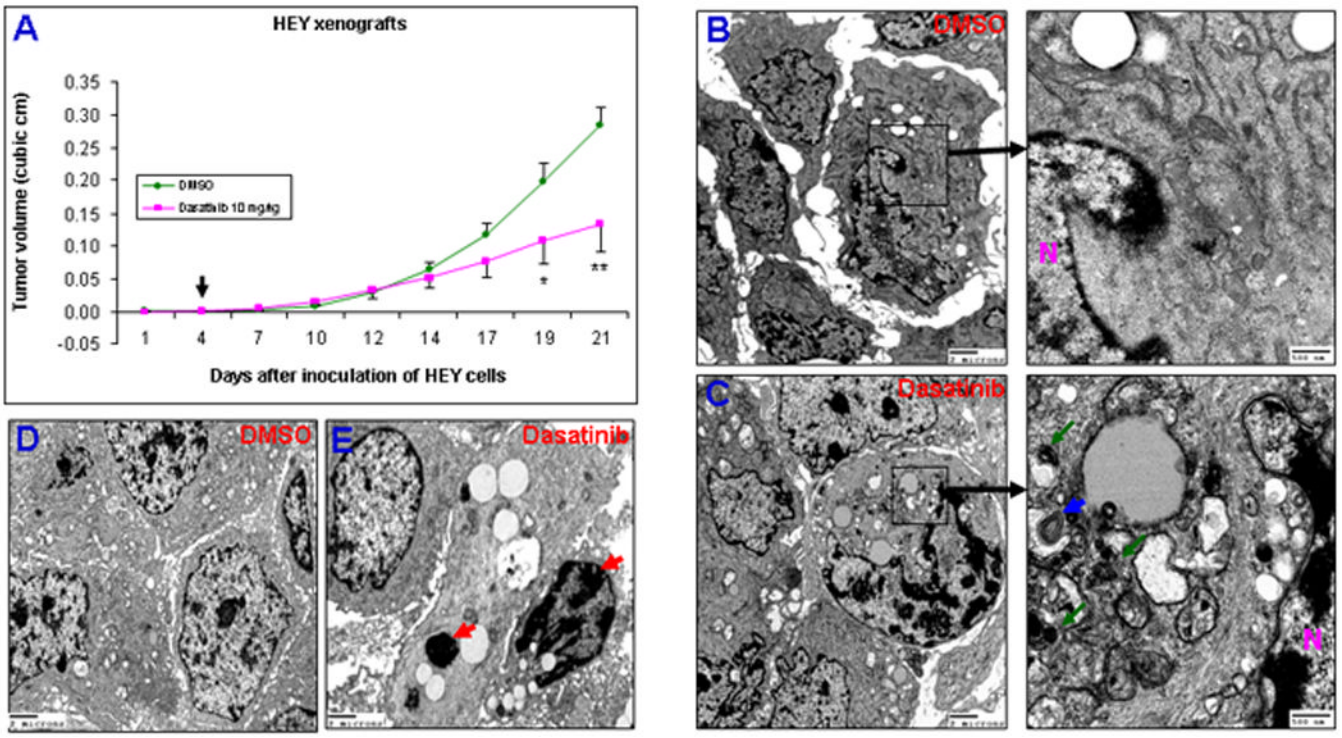

FIGURE 3.

Dasatinib inhibits ovarian tumor growth and induces autophagy and apoptosis in vivo. (**A**), Effect of dasatinib on tumor growth of HEY xenografts. The arrow indicates the beginning of dasatinib treatment. *, $P < 0.05$; **, $P < 0.01$ compared to DMSO-treated group. (**B**), Ultrastructural examination in DMSO-treated HEY xenograft tumors. Two magnifications (4,000 ×and 25,000 ×) of ultrastructure are shown. N indicates the nucleus. (**C**), Ultrastructural examination in dasatinib-treated HEY tumors. Two magnifications Autophagosomes are indicated by blue arrows and autophagolysomes by green arrows. (**D**), Ultrastructural examination in DMSO-treated HEY xenograft tumors. One magnification (4,000 ×) of ultrastructure is shown. (**E**), Ultrastructural examination in dasatinib-treated HEY xenograft tumors.

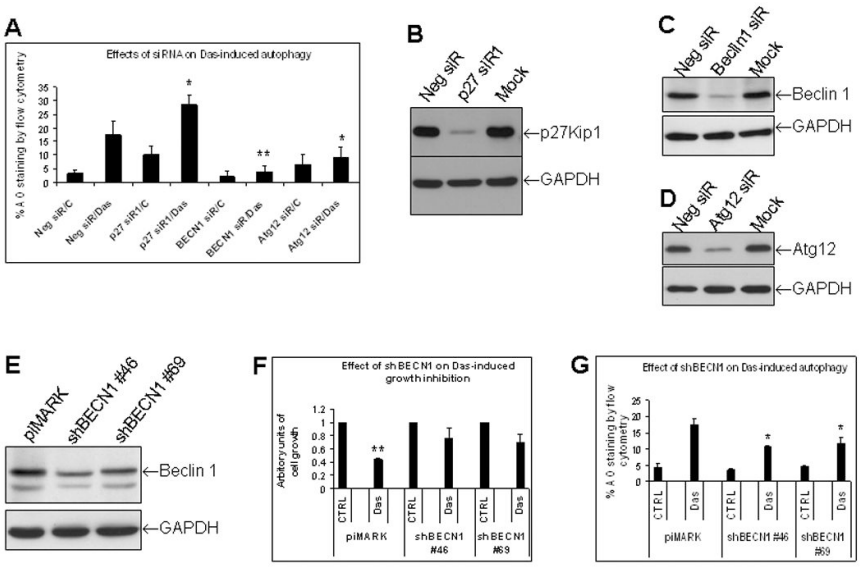

FIGURE 4.

Beclin 1 and Atg12, but not p27Kip1 are required for dasatinib-induced autophagy. Dasatinib-induced growth inhibition partially depends upon autophagy induction. (**A**), Effects of p27Kip1, Beclin 1 and Atg12 siRNAs on dasatinib (Das)-induced autophagy determined by AO staining. HEY cells were transfected with negative control (Neg siR), p27Kip1#1 (p27 siR1), Beclin 1 (BECN1 siR), or Atg12 (Atg siR) siRNAs (50 nM final concentration). Cells were treated either DMSO or Das for 24 hrs. AO staining was analyzed by flow cytometry. *, $P < 0.05$ compared to Neg siR/Das-treated group; **, $P < 0.01$ compared to Neg siR/Das-treated group. Data shown was averaged from 4 independent experiments (p27 siR data from 6 independent experiments). (**B–D**), Effect of p27Kip1, Beclin 1 and Atg12 siRNAs on their respective protein expression by Western blotting. Mock was the transfection reagent-treated cells. (**E**), Beclin 1 levels in stable subclones #46 and #69 that express Beclin 1 shRNA (shBECN1) detected by Western blotting. (**F**), Effects of shBECN1 on dasatinib-induced growth inhibition. HEY stable shBECN1 subclones #46 and #69 and their control piMARK cells were treated with Das (150 nM) for 72 hr. Cell viability was measured with crystal violet staining. DMSO-treated control (CTRL) was set as 1 for each subclone of piMARK, shBECN1#46 and shBECN1#69. Das-treated groups in these three subclones were expressed as ratio of respective CTRL. **, $P < 0.01$ compared to piMARK CTRL group. (**G**), Effects of shBECN1 on dasatinib-induced autophagy. shBECN1 subclones #46 and #69 and control piMARK cells were treated with Das for 24 hr and AO staining was performed.

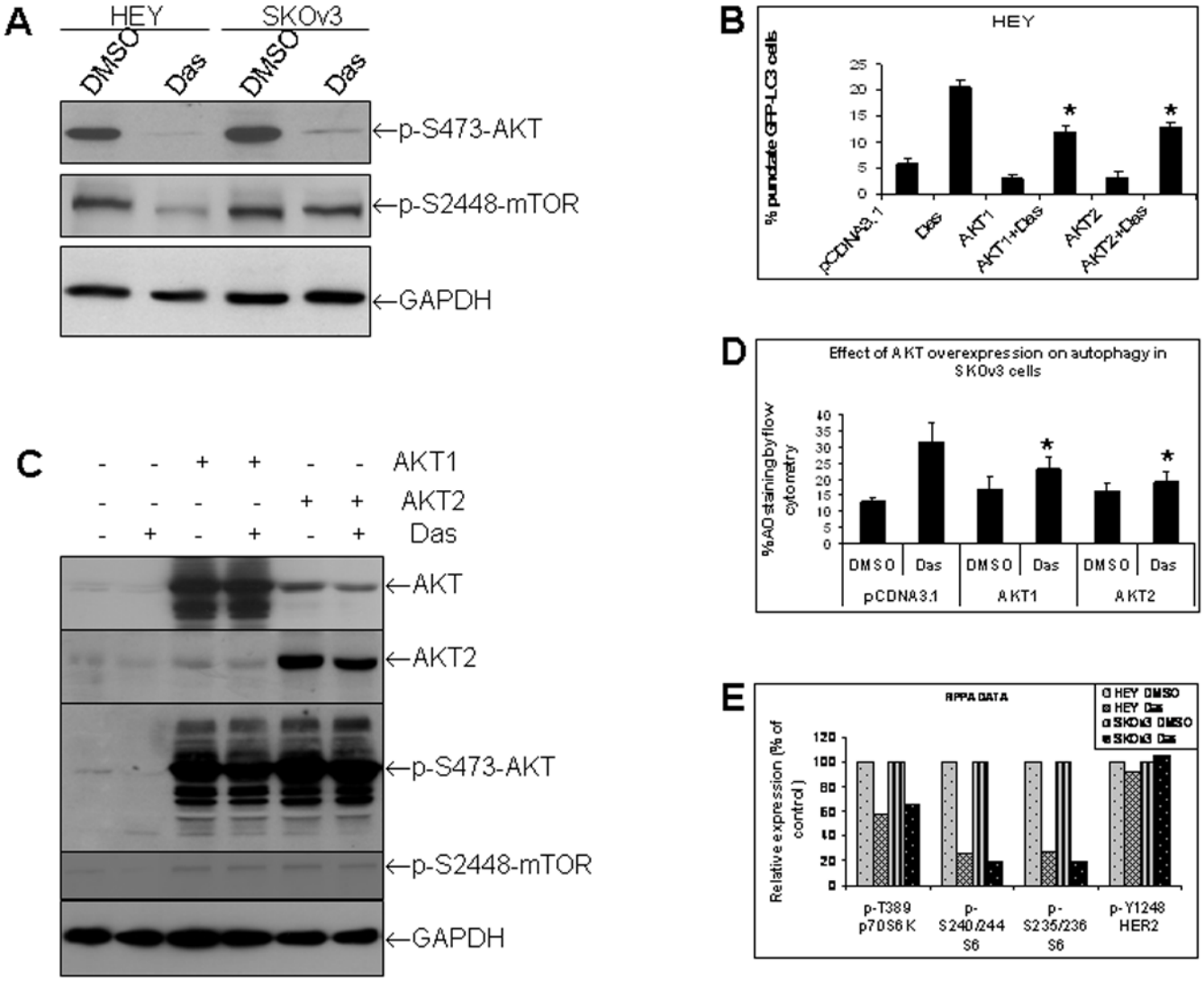

FIGURE 5.

Dasatinib-induced autophagy partially depends on AKT. (**A**), Effects of dasatinib (Das) on phosphorylation of AKT and mTOR as determined by Western blotting. (**B**), Effects of dominant positive AKT1 and AKT2 on Das-induced autophagy in HEY cells as determined by GFP-LC3 fluorescence microscopy. HEY cells were transiently co-transfected with AKT1, AKT2 and pGFP-LC3 for 48 hrs and then treated with dasatinib for another 24 hrs. *, $P < 0.05$ compared to Das-treated group. (**C**), AKT1, AKT2 and phosphorylation of AKT and mTOR expression was determined by Western blotting. (**D**), Effects of AKT1 and AKT2 on Das-induced autophagy in SKOv3 cells as determined by flow cytometric AO staining. SKOv3 cells were treated as described in (**B**). *, $P < 0.05$ compared to vector/Das-treated group (**E**), Effects of dasatinib on phosphorylaiton of p70S6K and S6 kinase determined by a reverse phase protein array (RPPA). phosphor-HER2 was used an internal control.

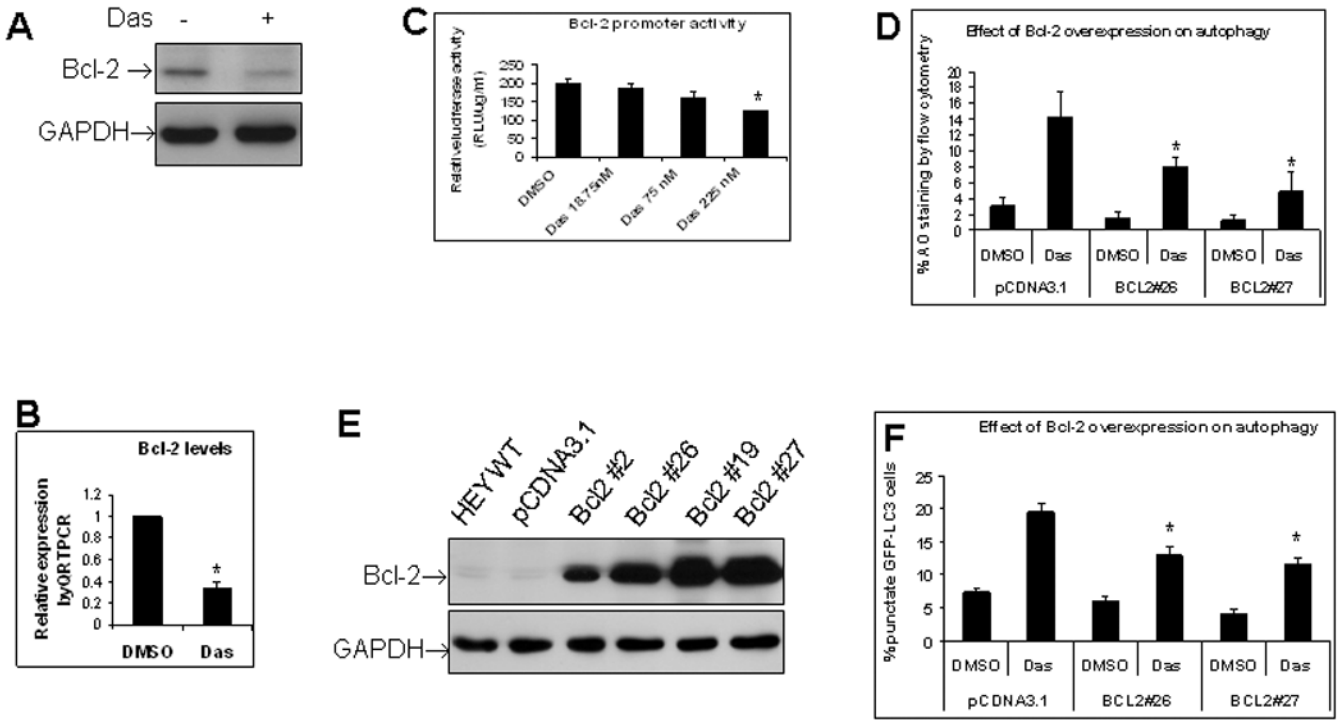

FIGURE 6.

Dasatinib-induced autophagy partially depends on Bcl-2. (**A**), Effect of dasatinib on Bcl-2 protein as detected by Western blotting. HEY cells were treated with dasatinib for 24 hrs. (**B**), Effect of dasatinib on Bcl-2 mRNA as detected by quantitative PCR. HEY cells were treated with dasatinib for 24 hrs. *, $p < 0.05$. (**C**), Effect of dasatinib on Bcl-2 promoter activity as detected by luciferase reporter assay. Relative luminescence units (RLU) were normalized with protein concentrations in each samples and final values of RLU were expressed as RLU per μg protein per ml. (**D**), Effect of Bcl-2 overexpression on dasatinib-induced autophagy as detected by AO staining. HEY Bcl-2 stable subclones #26 and #27 were treated with dasatinib for 24 hrs. AO staining was measured with flow cytometry. *, $p < 0.05$. (**F**), Effect of Bcl-2 overexpression on dasatinib-induced autophagy as determined by GFP-LC3 fluorescence microscopy. Bcl-2 stable sublines #26 and #27 were transiently transfected with pGFP-LC3 and then treated with dasatinib for another 24 hrs. *, $p < 0.05$. **, $p < 0.01$.